DOI: 10.1534/genetics.108.093534

glo-3, a Novel *Caenorhabditis elegans* Gene, Is Required for Lysosome-Related Organelle Biogenesis

Beverley M. Rabbitts,*,[1] Marcela K. Ciotti,†,[1] Natalie E. Miller,† Maxwell Kramer,* Andrea L. Lawrenson,† Steven Levitte,† Susan Kremer,* Elizabeth Kwan,* Allison M. Weis† and Greg J. Hermann*,†,[2]

**Program in Biochemistry and Molecular Biology and* †*Department of Biology, Lewis & Clark College, Portland, Oregon 97219*

Manuscript received July 9, 2008
Accepted for publication August 10, 2008

ABSTRACT

Gut granules are specialized lysosome-related organelles that act as sites of fat storage in *Caenorhabditis elegans* intestinal cells. We identified mutations in a gene, *glo-3*, that functions in the formation of embryonic gut granules. Some *glo-3(−)* alleles displayed a complete loss of embryonic gut granules, while other *glo-3(−)* alleles had reduced numbers of gut granules. A subset of *glo-3* alleles led to mislocalization of gut granule contents into the intestinal lumen, consistent with a defect in intracellular trafficking. *glo-3(−)* embryos lacking gut granules developed into adults containing gut granules, indicating that *glo-3(+)* function may be differentially required during development. We find that *glo-3(+)* acts in parallel with or downstream of the AP-3 complex and the PGP-2 ABC transporter in gut granule biogenesis. *glo-3* encodes a predicted membrane-associated protein that lacks obvious sequence homologs outside of nematodes. *glo-3* expression initiates in embryonic intestinal precursors and persists almost exclusively in intestinal cells through adulthood. GLO-3::GFP localizes to the gut granule membrane, suggesting it could play a direct role in the trafficking events at the gut granule. *smg-1(−)* suppression of *glo-3(−)* nonsense alleles indicates that the C-terminal half of GLO-3, predicted to be present in the cytoplasm, is not necessary for gut granule formation. Our studies identify GLO-3 as a novel player in the formation of lysosome-related organelles.

LYSOSOME-related organelles (LROs) comprise a functionally diverse set of cellular compartments. In mammals these organelles carry out specialized cellular functions including: storage and release of lung surfactant, secretion of blood clotting signals by α-granules, dense granules, and Weibel-Palade bodies, and pigment formation and storage by melanosomes (Raposo *et al.* 2007). Defects in the biogenesis of these and other LROs result in the human disease Hermansky–Pudlak syndrome (Wei 2006). While the functions of many LROs are well understood, there is comparatively much less known regarding the pathways and mechanisms that function in LRO formation.

Gut granules are newly defined LROs present within the intestinal cells of *C. elegans* (Hermann *et al.* 2005). Gut granules function as major sites for fat storage in *C. elegans* (Ashrafi *et al.* 2003; Schroeder *et al.* 2007). These organelles also store autofluorescent and birefringent materials (Babu 1974; Laufer *et al.* 1980), the identity and function of which are currently unknown. To investigate the mechanisms controlling LRO biogenesis we have identified a collection of mutants defective in gut granule biogenesis. Genes that can be mutated to give a Glo (*g*ut granule *lo*ss) phenotype (Hermann *et al.* 2005) include the Rab38 homolog GLO-1, the putative GLO-1 guanine nucleotide exchange factor GLO-4, the ABC transporter PGP-2, and subunits of the AP-3 and HOPS complexes (Hermann *et al.* 2005; Schroeder *et al.* 2007). Homologs of these genes function in the membrane trafficking steps mediating the biogenesis of mammalian and Drosophila LROs (Huizing *et al.* 2002; Ma *et al.* 2004; Cheong *et al.* 2006; Raposo *et al.* 2007), indicating that the cellular pathways controlling gut granule formation are evolutionarily conserved.

Here we present our phenotypic and molecular characterization of *glo-3*, a novel gene that functions in *Caenorhabditis elegans* gut granule biogenesis. We show that *glo-3* encodes a membrane-associated protein conserved in nematodes that localizes to the gut granule where it likely functions in trafficking to the compartment.

MATERIALS AND METHODS

***C. elegans* alleles and strains:** The wild-type strain N2 was used in our studies. All strains were grown at 22° unless otherwise noted. Strains were cultured as described (Brenner

[1]These authors contributed equally to this work.

[2]*Corresponding author:* Department of Biology, Lewis & Clark College, 0615 S.W. Palatine Hill Rd., Portland, OR 97219.
E-mail: hermann@lclark.edu

1974). Mutant alleles are listed by linkage group and references are listed at http://wormbase.org:

LGI: *apt-6(ok429)*, *dpy-5(e61)*, *fer-1(hc13ts)*, *pgp-2(kx48)*, *smg-1(r861)*.
LGII: *rrf-3(pk1426)*.
LGV: *dpy-11(e224)*, *glo-4(ok623)*.
LGX: *apt-7(tm920)*, *egl-15(n484)*, *glo-1(zu437)*, *glo-3(gm125)*, *glo-3(kx1)*, *glo-3(kx29)*, *glo-3(kx37)*, *glo-3(kx38)*, *glo-3(kx90)*, *glo-3(kx91)*, *glo-3(kx94)*, *glo-3(zu446)*, *unc-27(e159)*.
LG unknown: *pwIs50[lmp-1::gfp; unc-119(+)]* (Treusch *et al.* 2004), *pwIs72[vha-6$_p$::rab-5::gfp; unc-119(+)]* (Hermann *et al.* 2005), *pwIs87[vha-6$_p$::rme-1::gfp; unc-119(+)]* (Hermann *et al.* 2005), *pwIs170[vha-6$_p$::rab-7::gfp; unc-119(+)]* (Chen *et al.* 2006).
Extrachromosomal: *kxEx9[glo-1::gfp; rol-6(su1006)^p]* (Hermann *et al.* 2005), *kxEx41[glo-3::gfp; rol-6(su1006)^p]* (this work), *kxEx50[glo-3$_p$::gfp; rol-6(su1006)^p]* (this work).

Genetic manipulations: *glo-3* alleles were backcrossed to N2 at least two times prior to being used for phenotypic analysis. Initial complementation tests were performed by mating *glo(−)/ 0* males with *fer-1(hc13ts); glo-3(zu446)* hermaphrodites that were raised from embryogenesis through adulthood at 25°. At the nonpermissive temperature *fer-1(hc13ts)* animals do not produce functional sperm and are self-sterile (Ward and Miwa 1978), however mating with *fer-1(+); glo(−)* males results in the production of outcross progeny that were assessed for an embryonic Glo phenotype. To assess the embryonic Glo phenotype of class I/class II *glo-3* alleles, transheterozygotes were constructed by mating *glo-3(kx91)* and *glo-3(kx94)* males with both *fer-1(hc13ts); glo-3(zu446)* and *fer-1(hc13ts); glo-3(kx90)* self-sterile hermaphrodites and their progeny scored. To assess the embryonic Glo phenotype of class II/class III *glo-3* alleles, transheterozygotes were constructed by mating *glo-3(kx1)* and *glo-3(kx38)* males with both *fer-1(hc13ts); glo-3(zu446)* and *fer-1(hc13ts); glo-3(kx90)* self-sterile hermaphrodites and their progeny scored. The embryonic and adult Glo phenotypes exhibited by all the *glo-3* alleles were found to be recessive and expressed zygotically using standard genetic techniques. Maternal modification of the Glo phenotype was scored in the embryonic progeny of *glo-3(−)/+* hermaphrodites.

smg-1(r861); glo-3(−) animals were generated by mating *glo-3(−)* males with *smg-1(r861)* hermaphrodites. Dpy L1 progeny (Hermann *et al.* 2005) of the resulting transheterozygotes were isolated to select for *glo-3(−)* homozygotes. Adults in the next generation that displayed a protruding vulva were selected, as *smg-1(−)* homozygotes display this phenotype (Hodgkin *et al.* 1989). In all cases multiple double mutant lines were isolated and scored.

Double mutants of *glo-3(zu446)* with alleles of four other *glo* genes were constructed by taking unmarked *glo(−)* mutant males and mating them to *glo-3(−)* hermaphrodites containing tightly linked visible markers, including *dpy-5(e61)*, *dpy-11(e224)*, *egl-15(n484)*, and *unc-27(e159)*. Glo non-Dpy, Glo non-Egl, or Glo non-Unc F_2 progeny of this cross were isolated. Single Dpy, Egl, or Unc progeny were selected from the next generation and should be *glo* double mutants. At least two independent double-mutant lines were isolated from each cross, and in all cases they showed the same phenotype.

RNA interference (RNAi) was carried out by feeding using bacterial clones from a *C. elegans* RNAi library (Geneservice, Cambridge, UK) as described (Kamath *et al.* 2003). For *glo-3(RNAi)* experiments, the clone JA:F59F5.2 was used, which targets both *glo-3* and *glo-3short*. L1 stage larvae were placed on RNAi plates and scored as young adults.

Cloning *glo-3*: *glo-3* alleles were identified as described in Hermann *et al.* 2005. Three factor genetic crosses were used to map *glo-3(zu446)* to the *aex-2 egl-15* interval. *glo-3(kx90)*, *glo-3(kx94)*, and *glo-3(zu446)* were complemented by *nDf19*, indicating that *glo-3(+)* is not deleted by *nDf19*, similar to nearby genes *vab-3* and *daf-12*. SNP mapping with strain CB4856 placed *glo-3* in the interval defined by *snp_ZC504[1]* and *pkP6040* (mapping data are available upon request). RNAi of genes in this region identified F59F5.2/F59F5.8 as exhibiting an adult Glo phenotype similar to *glo-3(−)*. Of the eight cosmids spanning the interval, 3/7 stable transmitting lines injected with F59F5 at 10 ng/μl and 100 ng/μl of the co-injection marker pRF4[Rol-6^D] (Mello *et al.* 1991) rescued the embryonic Glo phenotype of *glo-3(zu446)*. The sequence of *glo-3* mutants was obtained by PCR amplifying the region spanning F59F5.2/F59F5.8 with Phusion high-fidelity DNA polymerase (New England Biolabs, Beverly, MA) from each of the mutant alleles. Amplifications and DNA sequencing (OHSU Core Facility) were performed in duplicate. Two cDNAs, yk1328a05 and yk571h2, encoded by *glo-3* have been previously described. The sequence for yk571h2 is known (GenBank AV190509 and AV17878) and corresponds to F59F5.2 (Wormbase WS180). We refer to this transcript as *glo-3short*. We completely sequenced yk1328a05 and found that it encodes a gene encompassing F59F5.2 and F59F5.8, which corresponds to an obsolete gene prediction F59F5.gc2 (Wormbase WS180). We refer to this transcript as *glo-3*. We verified the expression of *glo-3* and *glo-3short* in embryos and L4-stage animals by amplifying their corresponding cDNAs from total RNA isolated using Trizol/chloroform extraction. cDNA was generated using a d(T)20 primer with Superscript III (Invitrogen, Carlsbad, CA). In L4-stage animals the *glo-3* cDNA was amplified using P454 5′ ATGTTTGGTTATGTTGTTGT TAATGAAC 3′ and P456 5′ TTATTTTAACTGTTTTAACACG CATTC 3′ and the *glo-3short* cDNA was amplified with P454 and the nested primer P473 5′ TTCTACGTGTACAGAAGAACAA GAATC 3′ with the *glo-3short* 3′-UTR specific primer P455 5′ GTAGTGTAAACCATAATCAAAACTAAC 3′. In embryos, the *glo-3* cDNA was amplified with P472 5′ ACTGAATCGATTTG CACTTTTTAGCTG 3′ and P473 with the nested primer P404 5′ TCGTTAGATCACTTCAAGAAG 3′. The *glo-3short* cDNA was amplified from embryonic cDNA as described for L4's. A full-length *glo-3* cDNA was amplified with P457 5′ GGG GACAACTTTGTACAAAAAAGTTGTGTTTGGTTATGTTGT TGTTAATGAAC 3′ and P459 5′ GGGGACAACTTTGTACAA GAAAGTGTATTTTAACTGTTTTAACACGCATTC 3′ with Phusion DNA polymerase and Gateway (Invitrogen) cloned using a BP reaction into pDONR221. The *glo-3* cDNA sequence in the resulting pDONR221 plasmid was identical to yk1328a05 (GenBank FJ009048). The full-length *glo-3short* cDNA sequence was amplified with P457 and P458 5′ GGGGACAA CTTTGTACAAGAAAGTGTAGCATTTTGGGCTGTATGACAA TTTTC 3′ with Phusion DNA polymerase and Gateway cloned using a BP reaction into pDONR221. The resulting pDONR221-*glo-3* and pDONR221-*glo-3short* plasmids were sequenced to ensure a lack of PCR-generated mutations.

Generation of reporters: The transcriptional reporter *glo-3$_p$::gfp* was constructed using PCR fusion (Hobert 2002). A 1.6-kb sequence spanning from the predicted translational start of *glo-3* 5′ to the nearest upstream gene F59F5.1 was amplified using P411 5′ TCACTTTGCCTTCTGTGCGAGTTG 3′ and P412 5′ CAGTGAAAAGTTCTTCTCCTTTACTCATT TTGAACGAGTTTACCTGGAA 3′ from the cosmid F59F5. *gfp-nls* and flanking *unc-54* 3′-UTR was amplified from pPD95.67 (Addgene, Cambridge, MA) using P266 5′ AAGGGCCCGTA CGGCCGACTAGTAGG 3′ and P269 5′ ATGAGTAAAGGAGA AGAACTTTTCACTG 3′. P267 5′ GGAAACAGTTATGTTTG GTATATTGGG 3′and P413 5′ TCCAGATTAAAACGTCACA AGCAACCG 3′ were used in a PCR reaction that fused the *glo-3* promoter and *gfp-nls* sequences as described (Hobert 2002). The *glo-3$_p$::gfp-nls* reporter was co-injected into wild type at

6 ng/μl with pRF4[Rol-6^{D}] at 100 ng/μl. *kxEx50[glo-3$_p$::gfp; rol-6(su1006)^{D}]* was used for the analysis presented here, however five other independently derived lines showed similar GFP expression patterns.

The rescuing translational reporter GLO-3::GFP made using the *glo-3* genomic sequence was constructed using PCR fusion (Hobert 2002) by amplifying the genomic region containing the *glo-3* promoter and coding sequence from the cosmid F59F5 using P411 and P422 5′ AGTCGACCTGCAGG CATGCAAGCTTTTTAACTGTTTTAACACGCATTC 3′. The *gfp* coding sequence and flanking *unc-54* 3′-UTR was amplified from pPD95.75 (Addgene) using P399 5′ AGCTTGCATGC CTGCAGGTCGACT 3′ and P266. The two PCR products were fused using P413 and P267. The resulting *glo-3$_p$::glo-3::gfp* product was co-injected into *glo-3(zu446)* at 4.5 ng/μl with pRF4[Rol-6^{D}] at 100 ng/μl. *glo-3(zu446); kxEx41[glo-3::gfp; rol-6(su1006)^{D}]* was used in the analysis presented here, and six of six other independently derived lines showed a similar subcellular distribution of GFP. Seven of seven lines were Glo(+), showing wild-type patterns of birefringent material in embryos and autofluorescence in adults.

A second GLO-3::GFP rescuing translational reporter was made using the *glo-3* cDNA sequence, which was constructed by Gateway cloning *glo-3(cDNA)* from pDONR221-*glo-3* using an LR reaction into the *vha-6$_p$*::GTWY(Asp718)*::gfp* vector (Chen *et al.* 2006). The resulting plasmid has a C-terminal GFP fusion to GLO-3 and is regulated by the *vha-6* promoter. PCR fusion was used to place the *glo-3(cDNA)::gfp* sequence under the control of the *glo-3* promoter by amplifying the *glo-3* promoter and coding sequence from the cosmid F59F5 using P411 and P503 5′ GTTCATTAACAACAACATAACCAAACAT 3′. The *glo-3(cDNA)::gfp* coding sequence and flanking *unc-54* 3′-UTR was amplified from *vha-6$_p$::glo-3(cDNA)::gfp* using P454 and P500. The two PCR products were fused using P413 and P271 5′ GACTAGTTTTCCTTCCTCCTCTATAT 3′. The resulting *glo-3$_p$::glo-3(cDNA)::gfp* product was co-injected into *glo-3(kx90)* at 4.5 ng/μl with pRF4[Rol-6^{D}] at 100 ng/μl. Thirteen of 13 lines were Glo(+), showing wild-type patterns of birefringent material in embryos and autofluorescence in adults.

The translational reporter GLO-3short::GFP was constructed using PCR fusion by amplifying the genomic region containing the *glo-3* promoter and *glo-3short* coding sequence from the cosmid F59F5 using P411 and P440 5′ AGTC GACCTGCAGGCATGCAAGCTGCATTTTGGGCTGTATGAC AATTTTCG 3′. P440 contains a silent mutation that removes the 5′ splice site at the end of exon 4 without altering the amino acid sequence of GLO-3short. This ensures that the short isoform is produced. The *gfp* coding sequence and flanking *unc-54* 3′-UTR was amplified from pPD95.75 (Addgene) using P399 and P266. The two PCR products were fused using P413 and P267. The resulting *glo-3$_p$::glo-3short::gfp* product was co-injected into wild type at 5 ng/μl with pRF4[Rol-6^{D}] at 100 ng/μl. Eight of 8 independently derived lines showed a similar subcellular distribution of GFP.

The translational reporter GFP::GLO-3short was constructed using the *glo-3short* cDNA sequence by Gateway cloning *glo-3short* using an LR reaction into the *vha-6$_p$*::GTWY(*Eco*RI)::*gfp* vector (Chen *et al.* 2006). The resulting plasmid has an N-terminal GFP fusion to GLO-3short and is regulated by the *vha-6* promoter. PCR fusion was used to place the *gfp::glo-3short* sequence under the control of the *glo-3* promoter by amplifying the *glo-3* promoter and coding sequence from the cosmid F59F5 using P411 and P412. The *gfp::glo-3short* coding sequence and flanking *unc-54* 3′-UTR was amplified from *vha-6$_p$::gfp::glo-3short* using P269 and P500. The two PCR products were fused using P413 and P271 5′ GACTAGTTTTCCTTCCTCCTCTATAT 3′. The resulting *glo-3p::gfp::glo-3short(cDNA)* product was co-injected into wild type at 4.5 ng/μl with pRF4[Rol-6^{D}] at 100 ng/μl. Thirteen of 13 lines showed a similar subcellular distribution of GFP.

The translational reporter *glo-3$_p$*::GLO-3short was constructed using the *vha-6p::gfp::glo-3short* vector. PCR fusion was used to place the *glo-3short* sequence under the control of the *glo-3* promoter by amplifying the *glo-3* promoter and coding sequence from the cosmid F59F5 using P411 and P503. The *glo-3short* coding sequence and flanking *unc-54* 3′-UTR were amplified from *vha-6$_p$::gfp::glo-3short(cDNA)* using P454 and P500. The two PCR products were fused using P413 and P271. The resulting *glo-3$_p$::glo-3short(cDNA)* product was co-injected into *glo-3(kx90)* at 4.5 ng/μl with pRF4[Rol-6^{D}] at 100 ng/μl. Seven of seven lines showed embryonic and adult Glo phenotypes.

Microscopy: A Zeiss Axioskop II plus microscope (Thornwood, NY) equipped with DIC, polarization, and fluorescence optics was used for all light microscopy. Images were captured using a Diagnostic Instruments Insight Spot QE 4.1 digital camera with Spot Basic software (Sterling Heights, MI). Images were placed into separate channels in Photoshop 7.0 (Adobe, San Jose, CA) and analyzed for colocalization. Adults and larvae were immobilized prior to analysis by being mounted in 1× M9 containing 10 mm levamisole. Embryos that had developed beyond the 1.5-fold stage were visualized immediately after becoming hypoxic and immobilized due to the addition of excess *Escherichia coli* when the embryos were mounted. Intestinal autofluorescence in living animals was detected using the Zeiss 09 (Ex:BP450-490; Em:LP515), Zeiss 15 (Ex:BP586/12; Em:LP590), or custom (Ex:BP480/20; Em:BP530/20) fluorescence filters. Acidic compartments within intestinal cells were stained with Lysotracker Red (Molecular Probes, Eugene, OR) or acridine orange (Sigma, St. Louis) as described (Hermann *et al.* 2005). Fluid-phase endocytosis into adult intestinal cells was analyzed by feeding animals TRITC-dextran (Sigma) or TRITC-BSA (Sigma) using the procedures described by Hermann *et al.* 2005. Fat stores in living animals were stained with Nile Red (Molecular Probes) or BODIPY (493/503) (Molecular Probes) (Schroeder *et al.* 2007). Zeiss 15 and a custom (Ex:BP480/20; Em:BP530/20) fluorescence filter were used to analyze the colocalization of autofluorescence and vital staining in adult intestinal cells. Fat stores in fixed adults were stained with Sudan Black B (Sigma) as described (Ogg and Ruvkun 1998). Standard polarization optics were used to detect birefringent material in the embryonic intestine.

For immunostaining with affinity-purified rabbit FUS-1 (Kontani *et al.* 2005), RAB-5 (Audhya *et al.* 2007), PGP-2 (C-term) (Schroeder *et al.* 2007), VPS-27 (Roudier *et al.* 2005), and mouse 3E6 GFP antisera (Qbiogene), embryos (Leung *et al.* 1999) and adults (Currie *et al.* 2007) were fixed and stained as described. These protocols result in the loss of birefringent and autofluorescent gut granule contents.

RESULTS

***glo-3* alleles define three distinct gut granule phenotypes:** *glo-3* was identified in screens for *C. elegans* mutants defective in the formation and/or morphology of birefringent and autofluorescent gut granules (Hermann *et al.* 2005). We previously described *glo-3(zu446)* embryos as displaying a Glo phenotype [for a description of *C. elegans* embryogenesis see (Sulston *et al.* 1983)]. *glo-3(zu446)* is characterized by the mislocalization of birefringent material into the intestinal lumen, often

accompanied by the presence of one to five enlarged birefringent organelles in intestinal cells. *glo-3(zu446)* adults contain reduced numbers of autofluorescent compartments when compared to wild type (Hermann *et al.* 2005), and of the *glo* mutants characterized to date they display the highest number. Four other *glo-3* alleles (*gm125*, *kx29*, *kx37*, and *kx90*) were phenotypically indistinguishable from *glo-3(zu446)* (Hermann *et al.* 2005).

Continued genetic analysis of mutants in our collection of *glo* mutants led to the identification of four alleles of *glo-3* which were phenotypically distinct from *glo-3(zu446)*. *glo-3(kx91)* and *glo-3(kx94)* embryos mislocalized birefringent material into the embryonic intestinal lumen, however they completely lacked the one to five enlarged birefringent organelles often seen in *glo-3(zu446)* (Figure 1, D and F, Table 1). As adults, *glo-3(kx91)* and *glo-3(kx94)* typically lacked autofluorescent gut granules in anterior intestinal cells unlike *glo-3(zu446)*, which typically contained higher numbers (Figure 2D and Table 2). *glo-3(zu446)*, *glo-3(kx91)*, and *glo-3(kx94)* alleles contained similar numbers of autofluorescent compartments in posterior adult intestinal cells (Figure 2J and Table 2). On the basis of the different effects these alleles have on gut granule formation (Tables 1 and 2), we define *glo-3(kx91)* and *glo-3(kx94)* as *glo-3* class I alleles and *glo-3(gm125)*, *glo-3(kx29)*, *glo-3(kx37)*, *glo-3(kx90)*, and *glo-3(zu446)* as defining *glo-3* class II alleles.

Two alleles of *glo-3* were identified that rarely mislocalized birefringent material into the embryonic intestinal lumen. Instead, *glo-3(kx1)* and *glo-3(kx38)* embryos contained 5–30 enlarged birefringent organelles, which is reduced compared to wild type but substantially more than class II alleles (Figure 1, F and H; Table 1). In adult stages, *glo-3(kx1)*, *glo-3(kx38)*, and class II animals contained similar numbers of autofluorescent compartments (Table 2). Due to the unique embryonic phenotype displayed by *glo-3(kx1)* and *glo-3(kx38)* we define them as *glo-3* class III alleles.

Class I alleles likely cause the strongest *glo*-3 loss-of-function phenotype: We investigated which class of *glo-3* alleles exhibited the stronger phenotype. Unfortunately, *glo-3* is not deleted by *nDf19* (our unpublished observations), the only reported deletion spanning the *glo-3* genomic region, preventing an analysis of *glo-3(−)* phenotypic changes when individual alleles are placed over a deficiency. We therefore took a number of different approaches to investigate the relative severity of *glo-3(−)* alleles.

Often when two alleles that differentially affect gene function are placed in *trans*, the phenotype observed is that of the weaker allele (the allele that perturbs function the least). In four different *glo-3* class I/*glo-3* class II transheterozygous combinations we found that the class II embryonic phenotype was expressed (supplemental Table 1). We found in four different *glo-3* class II/*glo-3* class III transheterozygous combinations that the class III embryonic phenotype was expressed (supplemental Table 1). These data suggest that the relative strengths of *glo-3* alleles from strongest to weakest are class I > class II > class III.

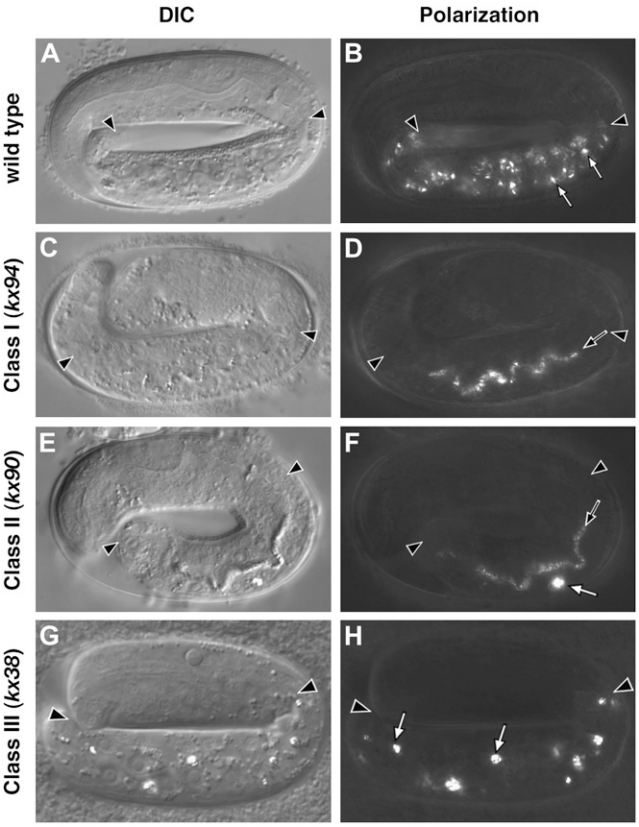

Figure 1.—Mutations in *glo-3* result in three different embryonic Glo phenotypes. (A and B) Birefringent gut granules (open arrows in B) were present within the intestinal cells of wild-type pretzel-stage embryos. (C and D) *glo-3(−)* alleles that exhibit a class I phenotype mislocalized birefringent material in the intestinal lumen (solid arrow in D) and did not contain birefringent material within embryonic intestinal cells. (E and F) *glo-3(−)* alleles that exhibit a class II phenotype mislocalized birefringent material in the intestinal lumen (solid arrow in F) and often contained a few enlarged birefringent granules (open arrow in E) within embryonic intestinal cells. (G and H) *glo-3(−)* alleles that exhibit a class III phenotype typically contained a reduced number of enlarged birefringent granules within embryonic intestinal cells (open arrows in H) and did not contain birefringent material within the intestinal lumen. Intestinal cells are located between the solid arrowheads in A–H. *C. elegans* embryos are ~50 μm in length.

We observed a maternal effect modification of the class I *glo-3* embryonic phenotype that further supports the idea that *glo-3* class I alleles exhibit a stronger phenotype than *glo-3* class II alleles. All of the *glo-3* alleles identified to date are strict recessive, zygotic effect for the Glo phenotype (Table 1 and data not shown). However, *glo-3(−)/glo-3(−)* class I progeny of *glo-3(+)/glo-3(−)* parents displayed a class II embryonic phenotype (Table 1). In contrast, *glo-3(−)/glo-3(−)* class I progeny of homozygous *glo-3(−)* class I parents display

TABLE 1

Birefringent gut granules in *glo-3(−)* embryos

Genotype	% of embryos that lacked birefringence in intestinal cells (% of embryos that also mislocalized birefringent material into the intestinal lumen)	% of embryos with 1–10 enlarged birefringent granules in intestinal cells (% of embryos that also mislocalized birefringent material into the intestinal lumen)	% of embryos with 11–30 enlarged birefringent granules in intestinal cells (% of embryos that also mislocalized birefringent material into the intestinal lumen)	*n*
Wild type[a]	0	0	0	52
Class I alleles			0	
glo-3(kx91)	100 (47)	0	0	77
glo-3(kx94)	100 (56)	0	0	107
Class II alleles			0	
glo-3(gm125)	41 (40)	59 (23)	0	83
glo-3(kx29)	41 (29)	59 (23)	0	73
glo-3(kx37)	68 (38)	32 (22)	0	69
glo-3(kx90)	47 (26)	53 (23)	0	115
glo-3(zu446)	54 (38)	46 (15)	0	125
Class III alleles				
glo-3(kx1)	0	12 (0)	88 (0)	91
glo-3(kx38)	0	25 (5)	75 (0)	92
		smg-1(−) suppression		
smg-1(r861)[b]	0	0	2 (0)	54
Class I alleles				
glo-3(kx91); smg-1(r861)	100 (94)	0	0	85
glo-3(kx94); smg-1(r861)	100 (63)	0	0	68
Class II alleles				
glo-3(gm125); smg-1(r861)	0	0	100 (0)	26
glo-3(kx29); smg-1(r861)	0	0	100 (0)	41
glo-3(kx37); smg-1(r861)	0	3 (100)	97 (0)	59
glo-3(kx90); smg-1(r861)	0	0	100 (0)	24
glo-3(zu446); smg-1(r861)	0	68 (6)	32 (0)	34
Class III alleles				
glo-3(kx1); smg-1(r861)	0	0	100 (0)	27
glo-3(kx38); smg-1(r861)	0	0	100 (0)	28
		Parental genotype[c]		
Class I alleles				
glo-3(kx91)/+	15 (9)	19 (11)	0	186
glo-3(kx94)/+	9 (4)	15 (9)	0	110
Class II alleles				
glo-3(kx90)/+	10 (6)	12 (6)	0	177
glo-3(zu446)/+	11 (4)	14 (3)	0	109

All strains were grown at 22°. Twofold and later-stage embryos were analyzed using polarization microscopy and scored for the presence, morphology, and localization of birefringent material in the intestine. *n*, number of embryos scored.

[a] Wild-type embryos contained >100 birefringent granules in intestinal cells and lacked birefringent material in the intestinal lumen.

[b] Ninety-eight percent of *smg-1(r861)* embryos contained >100 birefringent granules in intestinal cells and lacked birefringent material in the intestinal lumen.

[c] The progeny of heterozygous *glo-3(−)/+* hermaphrodites were scored. Twenty-five percent are predicted to be *glo-3(−)/glo-3(−)* and exhibit a Glo phenotype.

the class I phenotypes (Table 1). The phenotype of *glo-3(−)/glo-3(−)* class II mutants produced by *glo-3(+)/glo-3(−)* parents are unchanged relative to being produced by homozygous class II parents (Table 1). These results indicate that a wild-type maternal copy of *glo-3(+)* modifies the phenotype of class I alleles, making it more similar to the class II phenotype. One explanation of this observation is that class I alleles have less *glo-3(+)* activity than class II alleles, however with a contribution of wild-type *glo-3(+)* from the maternal parent *glo-3(class I)/glo-3(class I)* embryos have increased *glo-3(+)* activity and phenotypically resemble class II mutants.

Finally, the Glo phenotypes exhibited by the three classes of *glo-3* alleles suggest that class I alleles most compromise *glo-3* function. Class I mutants never contain birefringent gut granule contents within their intestinal

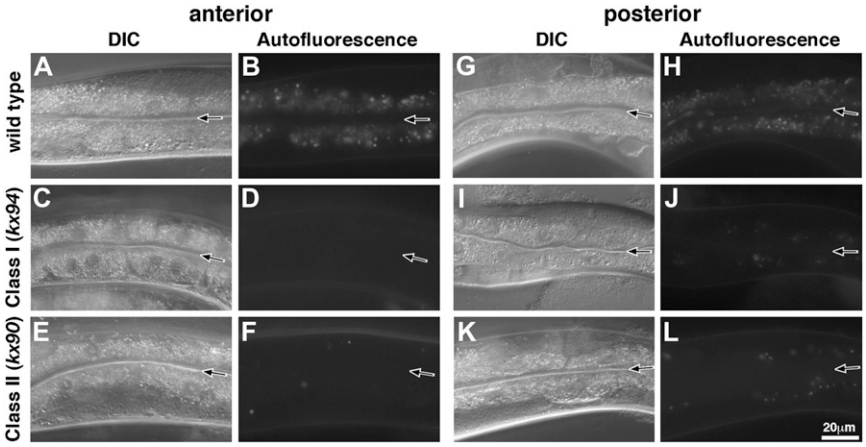

FIGURE 2.—Mutations in *glo-3* result in two distinct adult Glo phenotypes. Numerous autofluorescent gut granules visualized with a standard FITC filter were present within anterior (A and B) and posterior (G and H) intestinal cells of wild-type animals. *glo-3(−)* alleles that exhibit a class I phenotype lacked autofluorescent gut granules in anterior intestinal cells (C and D) and displayed substantially reduced numbers of autofluorescent organelles in posterior intestinal cells (I and J). *glo-3(−)* alleles that exhibit a class II phenotype contained substantially reduced numbers of autofluorescent organelles in both anterior (E and F) and posterior intestinal cells (K and L). The intestinal lumen is marked with a solid arrow in A–L.

cells (Table 1). In contrast, class II and class III mutants retain organelles with birefringent material, albeit at reduced numbers when compared to wild type (Figure 1). Class I mutant adults typically lack or have very few organelles with autofluorescent gut granule contents in anterior intestinal cells. Both class II and class III mutant adults display higher numbers of autofluorescent organelles (Table 2). Together, these data strongly suggest that *glo-3* class I alleles are more severe in their effect on gut granule biogenesis than either class II or class III alleles. We therefore present our phenotypic analysis of the class I allele *glo-3(kx94)*. We have also carried out a detailed phenotypic analysis of the autofluorescent organelles class II alleles *glo-3(kx90)* and *glo-3(zu446)* at the adult stage and not seen substantially different results than we present for the class I allele *glo-3(kx94)*.

***glo-3(−)* adults contain reduced numbers of gut granules:** The intestinal cells of wild-type adults contain hundreds of autofluorescent gut granules that are characterized by: (1) their acidification, (2) their function as terminal endocytic compartments, and (3) the presence of the gut granule membrane-associated ABC transporter PGP-2, and (4) the presence of fat (CLOKEY and JACOBSON 1986; SCHROEDER *et al.* 2007). To determine whether the reduction of autofluorescent intestinal compartments is reflective of a decrease in the number of gut granules, we examined *glo-3(kx94)* adults for organelles with gut granule characteristics. *glo-3(kx94)* adults contained substantially reduced numbers of acidified organelles marked by Lysotracker Red (Figure 3, A, B, G, and H) and acridine orange (supplemental Figure 1, C, D, I, and J). Similarly, reduced numbers of organelles in *glo-3(kx94)* adults were labeled with TRITC-dextran (Figure 3, C, D, I, and J) and TRITC-BSA (supplemental Figure 1, E, F, K, and L) that was endocytosed across the apical surface. Staining of fixed animals showed that reduced numbers of PGP-2-containing compartments were present within *glo-3(kx94)* adults (Figure 3, M and O). These results indicate that *glo-3(kx94)* adults contain reduced numbers of gut granules, indicative of defects in gut granule formation and/or stability.

We used three different labels, Nile Red, BODIPY 493/503, and Sudan Black, to mark fat-containing compartments in *glo-3(kx94)* adults. *glo-3(kx94)* animals fed Nile Red contained reduced numbers of stained compartments (Figure 3, F, K, and L). However, these compartments were only weakly stained when compared to wild type (data not shown). A similar loss of Nile Red staining was reported for *glo-3(RNAi)* in a genomewide screen for genes regulating *C. elegans* body fat levels (ASHRAFI *et al.* 2003). BODIPY 493/503-fed *glo-3(kx94)* animals completely lacked staining (supplemental Figure 1, A, B, G, and H). Our prior studies of a subset of *glo* mutants demonstrated that the loss of staining by vital stains such as Nile Red and BODIPY 493/503 did not correlate with a decrease in the overall fat content at the level of the organism (SCHROEDER *et al.* 2007). To investigate whether this might be the case in *glo-3(−)* animals, we fixed and stained *glo-3(kx94)* adults with Sudan Black, a sensitive marker for fat in *C. elegans* (KIMURA *et al.* 1997). *glo-3(kx94)* and wild-type animals displayed similar levels of Sudan Black staining (Figure 3, N and P). Consistent with our biochemical analysis of fat content in *glo* mutants that lack Nile Red staining (SCHROEDER *et al.* 2007), we did not observe a difference in Sudan Black staining between wild-type, *apt-7(tm920)*, *glo-1(zu437)*, and *pgp-2(kx48)* adults (supplemental Figure 2). These data show that Nile Red and BODPIY 493/503 only stain a subset of fat-containing organelles, namely gut granules, in *C. elegans* and strongly suggest that body fat levels are not dramatically altered in *glo-3(−)* adults.

The loss of gut granule-associated BODIPY 493/503 and reduced Nile Red staining in *glo-3(−)* animals raises the question of whether the autofluorescent gut granules present in *glo-3(−)* are properly formed. To address this issue, we analyzed whether the autofluorescent organelles in *glo-3(kx94)* adults contained gut granule-associated markers. Nearly all of the autofluorescent gut

TABLE 2

Autofluorescent gut granules in *glo-3(−)* adults

Genotype	% of animals with the specified no. of autofluorescent granules in anterior intestinal cells				% of animals with the specified no. of autofluorescent granules in posterior intestinal cells				Phenotype (anterior/posterior)	*n*
	Very low	Low	Medium	High	Very low	Low	Medium	High		
Wild type	0	0	0	100	0	0	1	99	High/high	89
glo-3(RNAi)[a]	0	100	0	0	0	85	5	0	Low/low	40
Class I alleles										
glo-3(kx91)	100	0	0	0	16	84	0	0	Very low/low	109
glo-3(kx94)	96	4	0	0	8	88	4	0	Very low/low	77
Class II alleles										
glo-3(gm125)	1	96	3	0	0	100	0	0	Low/low	77
glo-3(kx29)	23	77	0	0	0	99	1	0	Low/low	86
glo-3(kx37)	52	48	0	0	0	91	9	0	Low/low	67
glo-3(kx90)	23	77	0	0	0	96	4	0	Low/low	74
glo-3(zu446)	33	67	0	0	1	86	13	0	Low/low	95
Class III alleles										
glo-3(kx1)	2	83	12	3	0	50	45	5	Low/low	58
glo-3(kx38)	0	100	0	0	0	79	21	0	Low/low	71

All strains were grown at 22°. Individual young adults were analyzed using fluorescence microscopy with a fluorescein isothiocyanate (FITC) filter and were scored for the number of autofluorescent gut granules within the anterior and posterior areas of the intestine. Young animals were scored as very low when 0–5 autofluorescent gut granules were present, as low when 6–100 autofluorescent gut granules were present, as medium when 101–200 autofluorescent gut granules were present, and as high when >200 autofluorescent gut granules were present. *n*, number of animals scored.

[a] RNAi was carried out in the *rrf-3(pk1426)* RNAi-sensitive background (Simmer *et al.* 2003). Similar results were seen in the N2 strain.

granules in *glo-3(kx94)* were marked by Lysotracker Red and TRITC-BSA (supplemental Table 2); 62 and 69% of autofluorescent gut granules were stained by Nile Red and TRITC-dextran, respectively (supplemental Table 2). Due to experimental limitations we were unable to analyze the colocalization of autofluorescent material with acridine orange or anti-PGP-2 staining. However, similar numbers of autofluorescent, acridine orange-stained, and PGP-2-containing organelles were seen in *glo-3(kx94)* adults (Table 2 and supplemental Table 3). The formation of autofluorescent compartments in *glo-3(−)* adults required the activity of *glo-1* and *glo-4* (Table 3), two genes that function in gut granule biogenesis (Hermann *et al.* 2005). Together these data indicate that the autofluorescent organelles in *glo-3(−)* adults, with the exception of stored fat, appear to be indistinguishable from wild-type gut granules. The reduction/loss of vital staining for gut granule-associated fat could result from a *bona fide* defect in gut granule-associated fat accumulation or from alterations in trafficking to, or retention of Nile Red and BODIPY 493/503 in gut granules.

***glo-3(−)* embryos lack gut granules:** *glo-3(kx94)* embryos lack birefringent compartments in their intestinal cells and mislocalize birefringent material into the intestinal lumen (Figure 1, C and D). These phenotypes are consistent with *glo-3(kx94)* embryos being defective in gut granule biogenesis and lacking gut granules (Hermann *et al.* 2005). We investigated whether this was the case by staining with dyes and antibodies that label gut granules in wild-type embryos. Embryonic gut granules are acidified, fat-storing compartments that contain subunits of the V-ATPase, the Rab GTPase GLO-1, and PGP-2 (Hermann *et al.* 2005; Schroeder *et al.* 2007). Unlike wild type, *glo-3(kx94)* embryonic intestinal cells lacked acridine orange stained, acidified compartments (Figure 4, A and B). Consistent with the lack of acidification, FUS-1, an integral membrane-associated subunit of the V-ATPase (Kontani *et al.* 2005), was not detected in the intestinal cells of *glo-3(kx94)* embryos (Figure 4, G and H). Wild-type embryonic gut granules are stained by Nile Red and BODIPY 493/503 (Schroeder *et al.* 2007). Neither of these dyes stained compartments within intestinal cells of *glo-3(kx94)* embryos (Figure 4, D and F). In wild-type embryos, GLO-1::GFP localizes to gut granules (Hermann *et al.* 2005). GLO-1::GFP did not localize to any distinct organelles in the embryonic intestine of *glo-3(kx94)* (Figure 4L). We conclude that gut granules are lacking in *glo-3(kx94)* embryos and that embryonic gut granule biogenesis requires the function of *glo-3*.

We examined whether *glo-3(kx94)* embryos had defects in forming other endosomal organelles. The recycling endosome-associated protein RME-1::GFP (Grant *et al.* 2001), and early endosome-associated proteins RAB-5 (Audhya *et al.* 2007), RAB-5::GFP (Hermann *et al.* 2005), and VPS-27 (Roudier *et al.* 2005) had similar localizations and morphologies in

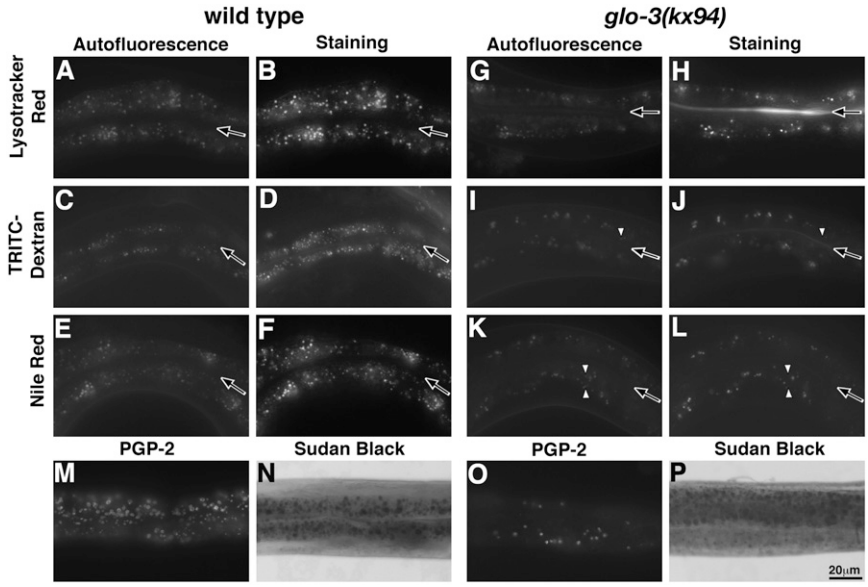

FIGURE 3.—*glo-3(−)* adults contain reduced numbers of gut granules. (A–F) In living animals, wild-type gut granules contained autofluorescent material (A, C, and E) that brightly stained with markers for acidity (B), terminal endocytic activity (D), and fat (F). In fixed wild-type adults, gut granules were marked by the PGP-2 protein (M). *glo-3(−)* adults contained dramatically reduced numbers of autofluorescent gut granules, the majority of which were acidified (H), terminal endocytic compartments (J), that contained fat (L). Nile Red staining of *glo-3(−)* adults was quite weak and its signal has been increased three to four times that in wild type to aid in its visualization. (O) *glo-3(−)* adults contained reduced numbers of PGP-2-stained organelles. A few autofluorescent compartments in *glo-3(−)* adults did not accumulate TRITC-dextran or Nile Red (open arrowheads in J and L). (N and P) Similar numbers of Sudan Black-stained organelles were present in wild-type and *glo-3(−)* adults. In A–L the intestinal lumen is marked with a solid arrow. Posterior intestinal cells are shown A–P.

wild-type and *glo-3(kx94)* embryonic intestinal cells (Figure 4, M–T). The localization of late endosome-associated proteins RAB-7::GFP and LMP-1::GFP (CHEN *et al.* 2006) was unchanged in *glo-3(kx94)* embryonic intestinal cells (Figure 4, U and V). However, as seen in two other *glo* mutants, *glo-1(−)* and *pgp-2(−)* (HERMANN *et al.* 2005; SCHROEDER *et al.* 2007), *glo-3(kx94)* embryos contained slightly enlarged LMP-1::GFP compartments (Figure 4, W and X). It is possible that LMP-1::GFP compartments become enlarged due to the mistrafficking of gut granule contents when there are defects in gut granule biogenesis (CURRIE *et al.* 2007). Our results show that many aspects of the endosomal system are properly organized in *glo-3(kx94)* embryonic intestinal cells, despite defects in gut granule formation.

***glo-3* encodes a novel predicted membrane-associated protein:** We mapped *glo-3* to a 220-kb interval defined by SNPs *snp_ZC504[1]* and *pkP6040*. An RNAi-based screen of genes in the interval identified RNAi clone JA:F59F5.2 as inducing an adult Glo phenotype very similar to *glo-3* class II and class III alleles (Table 2). JA:F59F5.2 targets two predicted genes, F59F5.2 and F59F5.8. Two previously isolated cDNAs, yk1328a05 and yk571h2, suggested that F59F5.2 and F59F5.8 are a single gene that is alternatively spliced to produce two transcripts. We independently isolated F59F5.2/.8 cDNAs from both adult and embryonic stages, supporting the conclusion that F59F5.2 and F59F5.8 are a single gene (see MATERIALS AND METHODS). We refer to the long F59F5.2/.8 transcript as *glo-3* and the F59F5.2 transcript as *glo-3short* (Figure 5A). *glo-3short* is generated by a lack of splicing at the 5′ end of intron 4. The Glo phenotypes of *glo-3(−)* were completely rescued by the cosmid F59F5 and by both *glo-3(genomic)::gfp* and *glo-3(cDNA)::gfp* expressed under the control of the *glo-3* promoter. DNA sequencing showed that all nine *glo-3* alleles had a mutation in the coding sequence of F59F5.2/.8 (Figure 5A).

glo-3 encodes a predicted protein that is conserved in nematodes, but lacks obvious sequence homologs in any other phyla (Figure 5B). The nematodes containing *glo-3*, including *C. elegans*, *C. briggsae*, and *C. remanei*, are known to be highly genetically divergent from one another (KIONTKE *et al.* 2004). GLO-3 is predicted to possess three membrane spanning domains and GLO-3short is predicted to possess two of these (Figure 5B). The likely topology of GLO-3 positions its 312-amino-acid C terminus in the cytoplasm. Extensive database searches did not reveal any other functional or structural motifs in the GLO-3 sequence.

GLO-3 is expressed in the intestine and associates with the gut granule membrane: Genes that mediate embryonic gut granule biogenesis begin to be expressed early in the developmental program of the intestine, typically during gastrulation of the two intestinal precursors (HERMANN *et al.* 2005; SCHROEDER *et al.* 2007). To determine whether this is the case for *glo-3*, we placed *gfp* under the transcriptional control of a 1.6-kb *glo-3* promoter fragment containing all of the sequences between the translational start sites of *glo-3* and the upstream gene F59F5.1. *glo-3$_p$::gfp* expression was first detected at gastrulation in the two intestinal precursors (Figure 6, A and B). *glo-3$_p$::gfp* continued to be expressed in the intestine through embryogenesis (Figure 6, C and D), larval stages (Figure 6, E and F), and into adulthood (Figure 6, G and H). Weak expression of *glo-3$_p$::gfp* was sometimes seen in a pair of cells in the head

TABLE 3

***glo-3(−)* double mutants**

Genotype	% of animals with the specified no. of autofluorescent granules in intestinal cells				
	None	Low	Medium	High	*n*
Wild type	0	0	0	100	24
glo-3(zu446)[a]	0	95	5	0	85
glo-1(zu437)	100	0	0	0	41
glo-4(ok623)[b]	100	0	0	0	32
pgp-2(kx48)[c]	0	3	97	0	35
apt-6(ok429)	16	84	0	0	19
glo-1(zu437) glo-3(zu446)	100	0	0	0	49
glo-4(ok623); glo-3(zu446)	100	0	0	0	95
pgp-2(kx48); glo-3(zu446)	100	0	0	0	54
apt-6(ok429); glo-3(zu446)	91	9	0	0	31

All strains were grown at 22°. Individual L4/young adults were analyzed using fluorescence microscopy with a fluorescein isothiocyanate (FITC) filter and were scored for the number of autofluorescent gut granules within the intestine. Animals were scored as none when autofluorescent gut granules were lacking, as low when 1–100 autofluorescent gut granules were present, as medium when 101–200 autofluorescent gut granules were present, and as high when >200 autofluorescent gut granules were present.

[a] The linked markers *egl-15(n484)* or *unc-27(e159)* did not alter the Glo phenotype of *glo-3(zu446)*. *n*, number of animals scored.

[b] The linked marker *dpy-11(e224)* did not alter the Glo phenotype of *glo-4(ok623)*.

[c] The linked marker *dpy-5(e61)* did not alter the Glo phenotype of *pgp-2(kx48)*.

with neuronal morphology and the intestinal valve cell (data not shown), which represented the only non-intestinal expression of *glo-3$_p$::gfp*.

We analyzed the localization of GLO-3 with a carboxy terminally tagged GLO-3::GFP fusion expressed under the control of the *glo-3* promoter. The GLO-3::GFP fusion fully rescued the embryonic and adult Glo phenotypes of *glo-3(zu446)* indicating that GLO-3::GFP is functional and likely localized properly. GLO-3::GFP had a punctate distribution within the intestinal primordium reminiscent of gut granules (Figure 7B). We compared the localization of GLO-3::GFP to the gut granule localized FUS-1 protein in fixed embryos and found that GLO-3::GFP was associated with gut granules from bean stage (Figure 7, A–D) through hatching (data not shown). The punctate distribution of GLO-3::GFP was lacking in *glo-1(−)* embryos (data not shown), which do not generate gut granules (Hermann *et al.* 2005). Furthermore, *apt-7(−)* and *pgp-2(−)* embryos, which contain reduced numbers of gut granules (Schroeder *et al.* 2007), lacked or displayed only a few GLO-3::GFP puncta, respectively (data not shown). In living embryos, GLO-3::GFP apparently localized to the limiting membrane of gut granules containing birefringent material (Figure 7, E–H). The association of GLO-3::GFP with the gut granule membrane is consistent with the prediction of three transmembrane segments within GLO-3. Moreover, the probable localization of GFP at the gut granule membrane in living embryos suggests that the carboxy terminus of GLO-3 is localized in the cytoplasm, as GFP fluorescence is quenched by low pH (Kneen *et al.* 1998), a well-defined characteristic of gut granules (Clokey and Jacobson 1986; Hermann *et al.* 2005).

To analyze the localization of GLO-3short we expressed GLO-3short carboxy (GLO3short::GFP) and amino terminal (GFP::GLO-3::short) GFP fusions under the control of the *glo-3* promoter. The GLO-3short GFP fusions did not localize to the gut granule membrane and instead were localized to the nuclear envelope or cytoplasm (data not shown). However, the GLO-3short GFP fusions and an untagged *glo-3short* cDNA expressed under control of the *glo-3* promoter did not rescue the Glo phenotype of *glo-3(−)* embryos or induce a dominant Glo phenotype when expressed in wild type. On the basis of these phenotypic data it is unclear whether the distribution we documented represents the *bona fide* localization of GLO-3short within intestinal cells.

***smg* suppression of *glo-3* alleles:** All of the *glo-3* alleles we have characterized contain premature stop codons, none of which are predicted to alter consensus splice sites (Blumenthal and Steward 1997). Due to the locations of the stop codons, the nonsense mediated RNA decay (NMD) pathway, encoded by the *smg* genes in *C. elegans* (Mango 2001; Maquat 2004), should target and degrade these *glo-3(−)* mRNAs, resulting in a similar Glo phenotype. It is therefore surprising that the nonsense alleles fall into three distinct phenotypic classes (Table 1 and Figure 5A). One possible explanation for the different phenotypes could be due to differential NMD of the *glo-3(−)* alleles, so that some alleles produce partially functional truncated GLO-3 proteins.

To test if the NMD pathway targets *glo-3* alleles and investigate whether the production of truncated GLO-3 might contribute to phenotypic differences between the alleles, we placed all nine *glo-3* alleles in the *smg-1(r861)* background. *smg-1* encodes a protein kinase essential for NMD in *C. elegans* (Grimson *et al.* 2004). *smg-1(−)* partially suppressed the embryonic Glo phenotype of all five class II *glo-3(−)* alleles (Table 1). When placed into the *smg-1(−)* background, class II alleles no longer mislocalized birefringent material into the intestinal lumen and displayed substantially increased numbers of birefringent gut granules so that they phenotypically resembled class III alleles (supplemental Figure 3 and Table 1), indicating that these alleles are targets for NMD. While *smg-1(−)* suppression did not result in wild-type numbers of gut granules, birefringent gut granules in *smg-1(r861); glo-3(zu446), smg-1(r861); glo-3(gm125),*

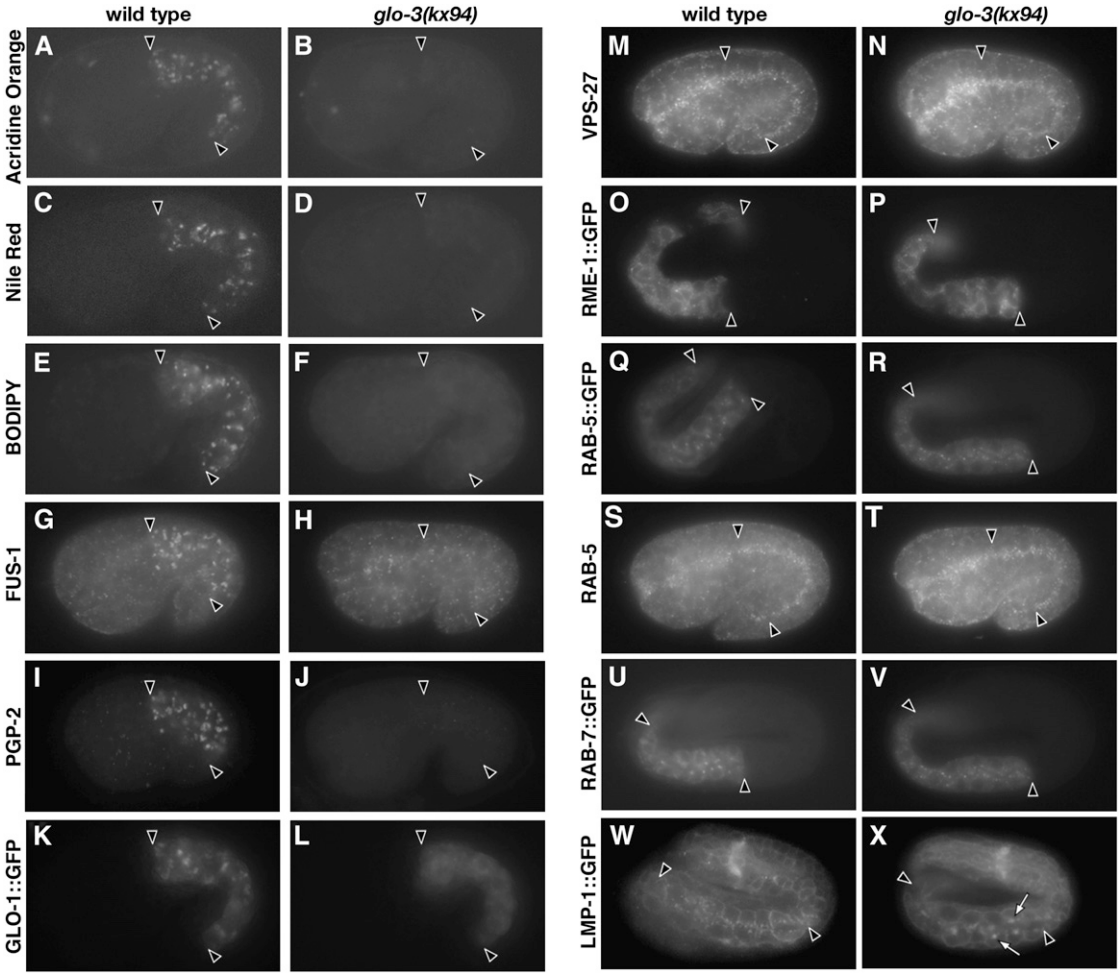

Figure 4.—*glo-3(−)* embryos lack gut granules but appear to contain other endosomal compartments. Acridine orange stained, acidified compartments present in wild-type 1.5-fold-stage embryos (A) were lacking in *glo-3(−)* embryos (B) Wild-type embryos displayed fat-containing, Nile Red and BODIPY 493/503-stained compartments (C and E) that were lacking in *glo-3(−)* embryos (D and F). Wild-type embryos contained anti-FUS-1 and anti-PGP-2 antibody marked compartments (G and I), which were not present in *glo-3(−)* embryos (H and J). GLO-1::GFP marked compartments present in wild-type (K) were lacking in *glo-3(−)* embryos (L). Antibodies that recognize VPS-27 and RAB-5 stained similar organelles in wild-type (M and S) and *glo-3(−)* (N and T) embryos. Anti-GFP antibodies used to stain embryos expressing RME-1, RAB-5, RAB-7, and LMP-1 fusion proteins showed similar staining patterns in wild-type (O, Q, U, and W) and *glo-3(−)* embryos (P, R, V, and X), with the exception that enlarged LMP-1::GFP marked organelles were present in *glo-3(−)* (open arrows in X). Intestinal cells are located between the solid arrowheads.

and *smg-1(r861); glo-3(kx29)* embryos were acidified, showing that they are likely properly formed compartments (data not shown). Notably, class I alleles, *kx91* and *kx94*, were not suppressed by *smg-1(−)* (Table 1), indicating that the truncated GLO-3 proteins produced by these alleles are not functional in gut granule biogenesis. The Glo phenotypes of both class III alleles were not substantially altered by *smg-1(−)* (Table 1), suggesting that they are not efficient targets of the SMG pathway, and produce truncated GLO-3 proteins with partial activity in the *smg-1(+)* background.

***glo-3* likely functions in parallel or downstream of the AP-3 complex and PGP-2:** Our prior studies have shown that AP-3 and PGP-2 function independently to promote the formation of gut granules in *C. elegans* (Schroeder *et al.* 2007). The AP-3 adapter complex in *C. elegans* is composed of four proteins, including the β3 subunit encoded by *apt-6* (Boehm and Bonifacino 2001). *pgp-2* encodes an ABC transporter, localized to the gut granule membrane, most similar to members of the ABCB subfamily of proteins that includes human P-glycoprotein, which mediates tumor multidrug resistance (Borst and Elferink 2002; Schroeder *et al.* 2007). Single AP-3 and *pgp-2(−)* null mutants display reduced numbers of gut granules in adults and embryos (Hermann *et al.* 2005; Schroeder *et al.* 2007), indicating that pathways for gut granule biogenesis are functioning in these mutants. On the basis of the severe Glo phenotype exhibited by *glo-3(−)*, it is unlikely that *glo-3(+)* functions upstream of AP-3 or *pgp-2(+)*. To determine whether *glo-3(+)* promotes gut granule formation in AP-3 or *pgp-2(−)* mutants, we introduced

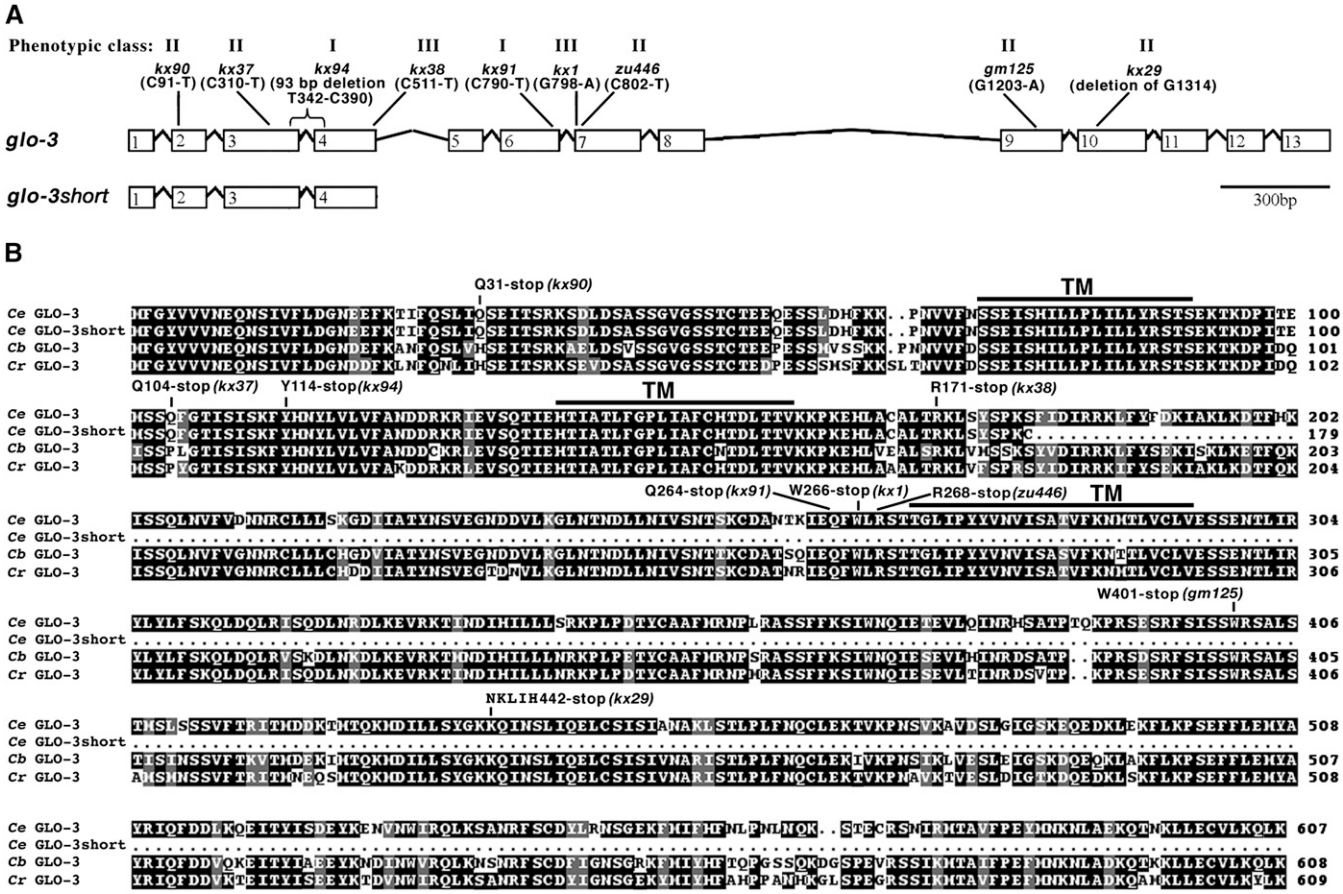

FIGURE 5.—Predicted structure of the *glo-3* gene and encoded protein. (A) The structure of the *glo-3* gene and the location and phenotypic class of mutations are shown. (B) The predicted protein sequences and alignment of GLO-3 from *C. elegans* (*Ce*), *C. briggsae* (*Cb*), and *C. remanei* (*Cr*). The location of predicted membrane-spanning domains (TM) identified using TMpred (HOFMANN and STOFFEL 1993) are shown.

glo-3(zu446) into *apt-6(−)* and *pgp-2(−)* genetic backgrounds. We found that *pgp-2(kx48); glo-3(zu446)* double mutants completely lacked autofluorescent organelles (Table 3). *apt-6(ok429); glo-3(zu446)* animals typically lacked and rarely contained very low numbers of autofluorescent compartments (Table 3). Both double mutants lacked birefringent compartments in embryos (data not shown). The phenotypes of the double mutants indicate that GLO-3 acts in parallel or downstream of AP-3 and PGP-2 in gut granule biogenesis.

DISCUSSION

***glo-3* alleles:** The nine *glo-3* alleles identified to date are nonsense alleles that fall into an allelic series with graded severity of embryonic and adult gut granule biogenesis phenotypes. Our phenotypic and genetic analyses strongly suggest that the relative mutant strengths are class I > class II > class III (Tables 1, 2, and supplemental Table 1). Surprisingly, the most 5′ allele *kx90*, which is predicted to severely truncate GLO-3, results in a class II phenotype. The most 3′ alleles, *gm125* and *kx29*, predicted to encode the longest GLO-3 mutant proteins also result in a class II phenotype. Class I alleles are flanked by class II alleles. In fact, three alleles, *kx91*, *kx1*, and *zu446*, located within a 12-nucleotide region, each display a distinct embryonic Glo phenotype (Figure 5). The complex relationships between genotype and phenotype suggest that alternative transcriptional start sites, alternative mRNA splicing, or nonsense mediated mRNA decay leading to the production of varied amounts of truncated GLO-3, may differentially affect *glo-3* alleles. These results, while not altering our conclusions as to the relative strength of *glo-3* alleles, prevent a definitive statement as to whether any of the alleles represent a *glo-3* null. Our conclusions regarding *glo-3* activity are based upon analysis of a class I mutant, which we believe contains a strong loss-of-function *glo-3* allele.

All five class II alleles are partially suppressed by mutations in *smg-1*, indicating that the nonsense mediated mRNA decay pathway targets their transcripts. Loss of this pathway is predicted to stabilize mRNAs with premature stop codons (MANGO 2001). The formation of gut granules in *smg-1(−); glo-3(zu446)* embryos indicates that the C-terminal half of GLO-3, which

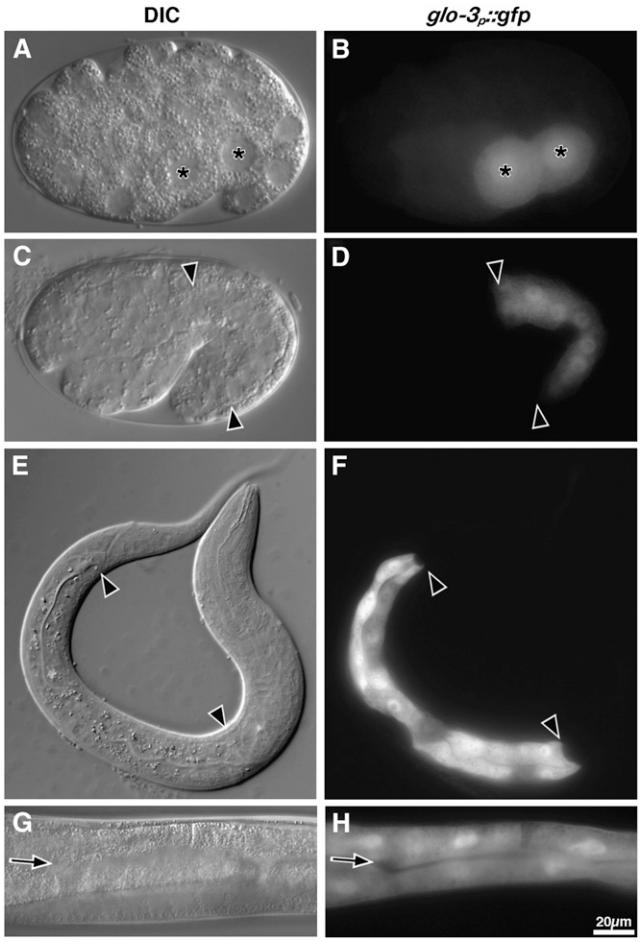

Figure 6.—*glo-3* is expressed in embryonic and adult intestinal cells. Strains carrying an extrachromosomal transgene in which the *glo-3* promoter drives the transcription of *gfp* (*glo-3$_p$::gfp*) resulted in the expression of *gfp* in intestinal precursors at the E^2 (A and B) and 1.5-fold stages (C and D). *gfp* was also expressed in the intestinal cells of L1 larvae (E and F) and adults (G and H). In A and B, the asterisks mark the nuclei of the two gastrulating intestinal precursors. In C–F, intestinal cells are located between the solid arrowheads. The solid arrows mark the intestinal lumen in G and H.

includes the third transmembrane domain and likely a large cytoplasmic domain, are not required for partial activity in gut granule biogenesis (Table 1). More surprisingly, *glo-3(kx90*) and *glo-3(kx37)* were partially suppressed by *smg-1(−)* (Table 1). These alleles are predicted to produce extremely truncated forms of GLO-3 (Figure 5). Rather than these truncated GLO-3 proteins being functional, we favor the possibility that low levels of alternative splicing or alternative translation initiation bypass the early stop codons and promote the formation of amino terminally truncated GLO-3 with partial activity. Our analysis of *glo-3(−); smg-1(−)* mutants strongly suggests that carboxy and possibly amino terminal domains of GLO-3 are not essential for its function in gut granule biogenesis; instead the region of GLO-3 containing transmembrane domains 2 and 3 appears to be critical for its activity.

***glo-3* function:** The *glo-3* locus encodes two transcripts, *glo-3* and *glo-3short*, which share the same predicted translational start site but differ at their 3′ ends due to alternative splicing and polyadenylation (Figure 5). The proteins encoded by these transcripts are identical for the first 178 amino acids; however, *glo-3* encodes a protein with an additional 427 amino acids at its carboxy terminus (Figure 5). We suggest that *glo-3short* does not significantly function in gut granule biogenesis. Five *glo-3* alleles disrupting gut granule biogenesis specifically affect *glo-3* and not *glo-3short* (Figure 5). The *glo-3short* cDNA expressed under control of the *glo-3* promoter did not rescue the Glo phenotypes of *glo-3(kx90)* (data not shown) indicating that expression of *glo-3short* is not sufficient to support gut granule biogenesis when *glo-3* function is compromised. Moreover, amino and carboxy terminal-tagged forms of GLO-3short were not localized to the gut granule membrane (data not shown).

In contrast to *glo-3short*, *glo-3* plays an essential role in the formation of embryonic gut granules. Our examination of six different markers that label embryonic gut granules failed to show any organelles with gut granule characteristics in *glo-3(kx94)* (Figure 4). *glo-3(+)* is likely to specifically function in gut granule formation as other endolysosomal organelles appeared to be properly formed in *glo-3(kx94)* embryos (Figure 4). Class I and class II alleles disrupting *glo-3* function result in the extracellular mislocalization of birefringent material into the embryonic intestinal lumen (Figure 1 and Table 1). Mutations affecting the function of factors with known roles in protein trafficking, such as GLO-1/Rab-38 and AP-3, result in the same phenotype (Hermann *et al.* 2005), suggesting that GLO-3 functions in trafficking to the embryonic gut granule. GLO-3 is likely positioned to play a direct role in the processes that regulate the formation, maturation, and/or stability of gut granules as a rescuing GLO-3::GFP fusion is localized to the gut granule membrane (Figure 7).

glo-3 clearly functions in the formation of adult gut granules, as they are lacking in anterior intestinal cells of class I alleles (Figure 2 and Table 2). Interestingly, *glo-3(kx94)* adults contained a significant number of autofluorescent organelles in posterior intestinal cells (Figure 2 and Table 2). These organelles appear to be gut granules, as they are acidified, terminal endocytic compartments (Figure 3 and supplemental Table 2), both defining gut granule characteristics (Clokey and Jacobson 1986), and *glo-1* and *glo-4*, two genes necessary for gut granule biogenesis (Hermann *et al.* 2005), are required for the formation of these compartments in *glo-3(−)* adults (Table 3). While the cellular basis of the anterior–posterior difference in the Glo phenotype is not known, there is clear precedent for differential gene expression along this axis in *C. elegans* intestinal cells (Schroeder and Mcghee 1998; Fukushige *et al.* 2005). We suggest that an additional factor or process that can

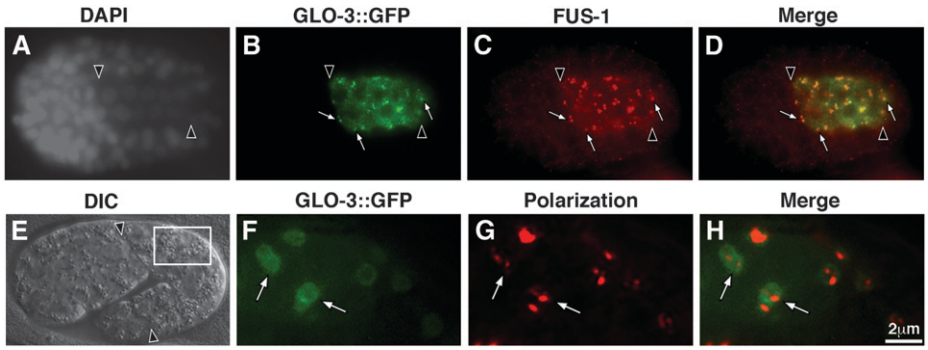

Figure 7.—GLO-3::GFP is localized to the gut granule membrane. (A–D) A bean-stage *glo-3(zu446)* embryo expressing GLO-3::GFP from the *glo-3* promoter showing colocalization of anti-GFP and anti-FUS-1 antibody staining at the same intestinal organelles (white arrows). (F–H) High magnification of the intestine of a GLO-3::GFP expressing 1.75-fold-stage embryo (white box in E). Birefringent material (pseudocolored red in G and H) is present within GLO-3::GFP-containing vesicles (white arrows in F–H). Intestinal cells are located between the black arrowheads in A–E.

functionally substitute for *glo-3* is expressed in posterior intestinal cells of larvae/adults.

The mechanisms that control gut granule formation in embryos and larvae/adults may be functionally distinct, as *glo-3(−)* class I embryos that lacked observable gut granules developed into adults that contained gut granules (Figures 1 and 2). The gut granules present in *glo-3(−)* adults might result from a *glo-3* independent pathway that functions exclusively in larvae/adults. However, it is also possible that both class I *glo-3* alleles we analyzed retain partial activity, which is sufficient to specifically promote gut granule formation in posterior intestinal cells of larvae/adults and not embryos.

The developmental pathway controlling the formation of birefringent gut granules in *C. elegans* embryos has long been known to be tightly coupled to endoderm fate specification (Laufer *et al.* 1980). A pathway involving Wnt signaling promotes the expression of two GATA transcription factors END-1/END-3 that induce gut cell fate and gut granule formation (Maduro 2006). These transcription factors promote the expression of genes at the E^2 stage, precisely when *glo-3* expression initiates (Figure 6), suggesting that *glo-3* may be a direct transcriptional target of END-1/END-3. *glo-3* joins *glo-1*, *pgp-2*, and *mrp-4*, genes with intestine restricted E^2 expression profiles that mediate the formation and differentiation of gut granules (Hermann *et al.* 2005; Currie *et al.* 2007; Schroeder *et al.* 2007). As such, gut granules provide an attractive and unique system to study the developmental pathways that control the cellular mechanisms that regulate the initiation of organelle formation and specialization.

Currently, we can only speculate as to the function of GLO-3 in gut granule formation. GLO-3 likely acts independently of the AP-3 complex and PGP-2 in the biogenesis of gut granules (Table 3). The lack of observable gut granules in *glo-3(−)* class I embryos is consistent with a role in membrane trafficking. However, GLO-3 is not homologous to known proteins involved in vesicle formation, movement, docking, and fusion. Alternatively, GLO-3 might function in the selection of cargo trafficked to the gut granule. *C. elegans* lacks obvious homologs of mannose-6-phosphate (Drickamer and Dodd 1999) and sortilin receptors (our unpublished results), the two best-characterized receptors for lysosomal cargo (Ghosh *et al.* 2003; Ni *et al.* 2006), indicating that the mechanisms in *C. elegans* selecting soluble lysosomal contents utilizes unidentified and possibly novel proteins. Recently, LIMP-2 a multipass lysosomal-associated protein was shown to act as a new type of sorting receptor for lysosomal cargo in mammalian cells (Reczek *et al.* 2007). While GLO-3 and LIMP-2 lack sequence homology, they have similar domain structures, raising the possibility that GLO-3 might function in the recognition of cargo trafficked to the gut granule. Testing this hypothesis awaits the identification of soluble gut granule-associated proteins.

Conservation of proteins controlling lysosome biogenesis: The proteins that mediate lysosome biogenesis are highly conserved in eukaryotes. The retromer, ESCRT, and HOPS protein complexes first identified as being necessary for trafficking to the yeast vacuole, a lysosomal equivalent, are well conserved and present in a broad range of metazoan taxa (Bowers and Stevens 2005). Similarly conserved are the vesicle coats, adapter complexes, phosphatidylinositol modifying enzymes, Rabs, and SNAREs that regulate cargo selection, vesicle budding, transport, and fusion within the endolysosomal system (Mullins and Bonifacino 2001). The formation of LROs requires many of the same highly conserved proteins required for lysosome biogenesis, including the AP-1, AP-3, and HOPS complexes (Raposo *et al.* 2007).

Studies of LRO biogenesis have led to the identification of proteins that function in organelle formation that are not as broadly conserved. Rab38/GLO-1, orthologs of which are not found in yeast (Pereira-Leal and Seabra 2001), are required for LRO biogenesis in *C. elegans* (Hermann *et al.* 2005), Drosophila (Ma *et al.* 2004), and mammals (Loftus *et al.* 2002; Wasmeier *et al.* 2006). Eight proteins composing the BLOC-1 and BLOC-2 complexes that function in LRO biogenesis in mammals (Raposo *et al.* 2007), are found only in metazoans (Dell'angelica 2004). Nearly all of the subunits of the BLOC-1 and BLOC-2 complexes are conserved in Drosophila, where at least one subunit is

necessary for the biogenesis of a LRO (Falcon-Perez *et al.* 2007; Syrzycka *et al.* 2007). Notably, few BLOC-1 or BLOC-2 subunits are obviously conserved in *C. elegans* (De Voer *et al.* 2008).

GLO-3 is unique among factors functioning in LRO biogenesis, being present in only one group of organisms. Extensive searches failed to identify any proteins outside nematodes with sequence similarity to GLO-3. It is possible that proteins functionally homologous to GLO-3 have significantly diverged so as not to be detectable. Alternatively, nematodes may have evolved a novel mechanism involving GLO-3 that mediates the assembly of lysosome-related organelles. Future studies aimed at identifying the molecular function of GLO-3 should resolve this issue.

We gratefully acknowledge members of the Hermann, Binford, Lycan, and Reiness laboratories for advice. We thank Anjon Audhya, Barth Grant, Yuji Kohara, Kenji Kontani, and Renaud Legouis for gifts of strains, antisera, and plasmids. Some nematode strains were provided by the *Caenorhabditis* Genetics Center, the *C. elegans* Knockout Consortium, and the National Bioresource Project for *C. elegans*. We thank Karen Kelly for genetic characterization of class I *glo-3* alleles. This work was supported by grants from the National Science Foundation (MCB-0314332 and MCB-0716280), the John S. Rogers Summer Research Program, and the M. J. Murdock Charitable Trust.

LITERATURE CITED

Ashrafi, K., F. Y. Chang, J. L. Watts, A. G. Fraser, R. S. Kamath *et al.*, 2003 Genome-wide RNAi analysis of *Caenorhabditis elegans* fat regulatory genes. Nature **421:** 268–272.

Audhya, A., A. Desai and K. Oegema, 2007 A role for Rab5 in structuring the endoplasmic reticulum. J. Cell Biol. **178:** 43–56.

Babu, P., 1974 Biochemical genetics of *Caenorhabditis elegans*. Mol. Gen. Genet. **135:** 39–44.

Blumenthal, T., and K. Steward, 1997 RNA processing and gene structure, pp. 117–145 in *C. elegans II*, edited by D. L. Riddle, T. Blumenthal, B. J. Meyer and J. R. Priess. Cold Spring Harbor Laboratory Press, Plainview, NY.

Boehm, M., and J. S. Bonifacino, 2001 Adaptins: the final recount. Mol. Biol. Cell **12:** 2907–2920.

Borst, P., and R. O. Elferink, 2002 Mammalian ABC transporters in health and disease. Annu. Rev. Biochem. **71:** 537–592.

Bowers, K., and T. H. Stevens, 2005 Protein transport from the late Golgi to the vacuole in the yeast *Saccharomyces cerevisiae*. Biochim. Biophys. Acta **1744:** 438–454.

Brenner, S., 1974 The genetics of *Caenorhabditis elegans*. Genetics **77:** 71–94.

Chen, C. C., P. J. Schweinsberg, S. Vashist, D. P. Mareiniss, E. J. Lambie *et al.*, 2006 RAB-10 is required for endocytic recycling in the *Caenorhabditis elegans* intestine. Mol. Biol. Cell **17:** 1286–1297.

Cheong, N., M. Madesh, L. W. Gonzales, M. Zhao, K. Yu *et al.*, 2006 Functional and trafficking defects in ATP binding cassette A3 mutants associated with respiratory distress syndrome. J. Biol. Chem. **281:** 9791–9800.

Clokey, G. V., and L. A. Jacobson, 1986 The autofluorescent "lipofuscin granules" in the intestinal cells of *Caenorhabditis elegans* are secondary lysosomes. Mech. Ageing Dev. **35:** 79–94.

Currie, E., B. King, A. L. Lawrenson, L. K. Schroeder, A. M. Kershner *et al.*, 2007 Role of the *Caenorhabditis elegans* multidrug resistance gene, *mrp-4*, in gut granule differentiation. Genetics **177:** 1569–1582.

de Voer, G., D. Peters and P. E. Taschner, 2008 *Caenorhabditis elegans* as a model for lysosomal storage disorders. Biochim. Biophys. Acta **1782:** 433–446.

Dell'Angelica, E. C., 2004 The building BLOC(k)s of lysosomes and related organelles. Curr. Opin. Cell Biol. **16:** 458–464.

Drickamer, K., and R. B. Dodd, 1999 C-type lectin-like domains in *Caenorhabditis elegans*: predictions from the complete genome sequence. Glycobiology **9:** 1357–1369.

Falcon-Perez, J. M., R. Romero-Calderon, E. S. Brooks, D. E. Krantz and E. C. Dell'Angelica, 2007 The *Drosophila* pigmentation gene pink (p) encodes a homologue of human Hermansky-Pudlak syndrome 5 (HPS5). Traffic **8:** 154–168.

Fukushige, T., B. Goszczynski, J. Yan and J. D. McGhee, 2005 Transcriptional control and patterning of the pho-1 gene, an essential acid phosphatase expressed in the C. elegans intestine. Dev. Biol. **279:** 446–461.

Ghosh, P., N. M. Dahms and S. Kornfeld, 2003 Mannose 6-phosphate receptors: new twists in the tale. Nat. Rev. Mol. Cell. Biol. **4:** 202–212.

Grant, B., Y. Zhang, M.-C. Paupard, S. X. Lin, D. Hall *et al.*, 2001 Evidence that RME-1, a conserved *C. elegans* EH domain protein, functions in endocytic recycling. Nat. Cell Biol. **3:** 573–579.

Grimson, A., S. O'Connor, C. L. Newman and P. Anderson, 2004 SMG-1 is a phosphatidylinositol kinase-related protein kinase required for nonsense-mediated mRNA decay in *Caenorhabditis elegans*. Mol. Cell. Biol. **24:** 7483–7490.

Hermann, G. J., L. K. Schroeder, C. A. Hieb, A. M. Kershner, B. M. Rabbitts *et al.*, 2005 Genetic analysis of lysosomal trafficking in *Caenorhabditis elegans*. Mol. Biol. Cell **16:** 3273–3288.

Hobert, O., 2002 PCR fusion-based approach to create reporter gene constructs for expression analysis in transgenic *C. elegans*. BioTechniques **32:** 728–730.

Hodgkin, J., A. Papp, R. Pulak, V. Ambros and P. Anderson, 1989 A new kind of informational suppression in the nematode *Caenorhabditis elegans*. Genetics **123:** 301–313.

Hofmann, K., and W. Stoffel, 1993 TMBASE: a database of membrane spanning protein segments. Biol. Chem. Hoppe-Seyler **374:** 166.

Huizing, M., R. E. Boissy and W. A. Gahl, 2002 Hermansky-Pudlak syndrome: vesicle formation from yeast to man. Pigment Cell Res. **15:** 405–419.

Kamath, R. S., A. G. Fraser, Y. Dong, G. Poulin, R. Durbin *et al.*, 2003 Systematic functional analysis of the *Caenorhabditis elegans* genome using RNAi. Nature **421:** 231–237.

Kimura, K. D., H. A. Tissenbaum, Y. Liu and G. Ruvkun, 1997 *daf-2*, an insulin receptor-like gene that regulates longevity and diapause in *Caenorhabditis elegans*. Science **277:** 942–946.

Kiontke, K., N. P. Gavin, Y. Raynes, C. Roehrig, F. Piano *et al.*, 2004 *Caenorhabditis* phylogeny predicts convergence of hermaphroditism and extensive intron loss. Proc. Natl. Acad. Sci. USA **101:** 9003–9008.

Kneen, M., J. Farinas, Y. Li and A. S. Verkman, 1998 Green fluorescent protein as a noninvasive intracellular pH indicator. Biophys. J. **74:** 1591–1599.

Kontani, K., I. P. G. Moskowitz and J. H. Rothman, 2005 Repression of cell-cell fusion by components of the *C. elegans* vacuolar ATPase complex. Dev. Cell **8:** 787–794.

Laufer, J. S., P. Bazzicalupo and W. B. Wood, 1980 Segregation of developmental potential in early embryos of *Caenorhabditis elegans*. Cell **19:** 569–577.

Leung, B., G. J. Hermann and J. R. Priess, 1999 Organogenesis of the *Caenorhabditis elegans* intestine. Dev. Biol. **216:** 114–134.

Loftus, S. K., D. M. Larson, L. L. Baxter, A. Antonellis, Y. Chen *et al.*, 2002 Mutation of melanosome protein RAB38 in *chocolate* mice. Proc. Natl Acad. Sci. USA **99:** 4471–4476.

Ma, J., H. Plesken, J. E. Treisman, I. Edelman-Novemsky and M. Ren, 2004 Lightoid and Claret: A rab GTPase and its putative guanine nucleotide exchange factor in biogenesis of Drosophila eye pigment granules. Proc. Natl. Acad. Sci. USA **101:** 11652–11657.

Maduro, M. F., 2006 Endomesoderm specification in *Caenorhabditis elegans* and other nematodes. BioEssays **28:** 1010–1022.

Mango, S. E., 2001 Stop making nonSense: the *C. elegans smg* genes. Trends Genet. **17:** 646–653.

Maquat, L. E., 2004 Nonsense-mediated mRNA decay: splicing, translation and mRNP dynamics. Nat. Rev. Mol. Cell Biol. **5:** 89–99.

Mello, C. C., J. M. Kramer, D. Stinchcomb and V. Ambros, 1991 Efficient gene transfer in *C.elegans*: extrachromosomal maintenance and integration of transforming sequences. EMBO J. **10:** 3959–3970.

Mullins, C., and J. S. Bonifacino, 2001 The molecular machinery for lysosome biogenesis. BioEssays **23:** 333–343.

Ni, X., M. Canuel and C. R. Morales, 2006 The sorting and trafficking of lysosomal proteins. Histol. Histopathol. **21:** 899–913.

Ogg, S., and G. Ruvkun, 1998 The *C. elegans* PTEN homolog, DAF-18, acts in the insulin receptor-like metabolic signaling pathway. Mol. Cell **2:** 887–893.

Pereira-Leal, J. B., and M. C. Seabra, 2001 Evolution of the Rab family of small GTP-binding proteins. J. Mol. Biol. **313:** 889–901.

Raposo, G., M. S. Marks and D. F. Cutler, 2007 Lysosome-related organelles: driving post-Golgi compartments into specialisation. Curr. Opin. Cell Biol. **19:** 394–401.

Reczek, D., M. Schwake, J. Schroder, H. Hughes, J. Blanz *et al.*, 2007 LIMP-2 is a receptor for lysosomal mannose-6-phosphate-independent targeting of beta-glucocerebrosidase. Cell **131:** 770–783.

Roudier, N., C. Lefebvre and R. Legouis, 2005 CeVPS-27 is an endosomal protein required for the molting and the endocytic trafficking of the low-density lipoprotein receptor-related protein 1 in *Caenorhabditis elegans*. Traffic **6:** 695–705.

Schroeder, D. F., and J. D. McGhee, 1998 Anterior-posterior patterning within the *Caenorhabditis elegans* endoderm. Development **125:** 4877–4887.

Schroeder, L. K., S. Kremer, M. J. Kramer, E. Currie, E. Kwan *et al.*, 2007 Function of the *Caenorhabditis elegans* ABC transporter PGP-2 in the biogenesis of a lysosome-related fat storage organelle. Mol. Biol. Cell **18:** 995–1008.

Simmer, F., C. Moorman, A. M. van der Linden, E. Kuijk, P. V. van den Berghe *et al.*, 2003 Genome-wide RNAi of *C. elegans* using the hypersensitive rrf-3 strain reveals novel gene functions. PLoS Biol. **1:** E12.

Sulston, J. E., E. Schierenberg, J. G. White and J. N. Thomson, 1983 The embryonic cell lineage of the nematode *Caenorhabditis elegans*. Dev. Biol. **100:** 64–119.

Syrzycka, M., L. A. McEachern, J. Kinneard, K. Prabhu, K. Fitzpatrick *et al.*, 2007 The pink gene encodes the Drosophila orthologue of the human Hermansky-Pudlak syndrome 5 (HPS5) gene. Genome **50:** 548–556.

Treusch, S., S. Knuth, S. A. Slaugenhaupt, E. Goldin, B. D. Grant *et al.*, 2004 *Caenorhabditis elegans* functional orthologue of human protein h-mucolipin-1 is required for lysosome biogenesis. Proc. Natl. Acad. Sci. USA **13:** 4483–4488.

Ward, S., and J. Miwa, 1978 Characterization of temperature-sensitive, fertilization-defective mutants of the nematode *Caenorhabditis elegans*. Genetics **88:** 285–303.

Wasmeier, C., M. Romao, L. Plowright, D. C. Bennett, G. Raposo *et al.*, 2006 Rab38 and Rab32 control post-Golgi trafficking of melanogenic enzymes. J. Cell Biol. **175:** 271–281.

Wei, M. L., 2006 Hermansky-Pudlak syndrome: a disease of protein trafficking and organelle function. Pigment Cell Res. **19:** 19–42.

Communicating editor: D. I. Greenstein